JACS
JOURNAL OF THE AMERICAN CHEMICAL SOCIETY

Article

pubs.acs.org/JACS

Metal–Organic Polyhedron Capped with Cucurbit[8]uril Delivers Doxorubicin to Cancer Cells

Soumen K. Samanta,[†] Damien Moncelet,[‡] Volker Briken,*[,‡] and Lyle Isaacs*[,†]

[†]Department of Chemistry and Biochemistry and [‡]Department of Cell Biology and Molecular Genetics, University of Maryland, College Park, Maryland 20742, United States

Supporting Information

ABSTRACT: Self-assembly of ligand **1** and $Pd(NO_3)_2$ delivers Fujita-type metal–organic polyhedron (MOP) **3** which bears 24 covalently attached methyl viologen units on its external surface, as evidenced by ^{1}H NMR, diffusion-ordered spectroscopy NMR, electrospray mass spectrometry, transmission electron microscopy, and atomic force microscopy measurements. MOP **3** undergoes noncovalent complexation with cucurbit[*n*]urils to yield MOPs **4**–**6** with diameter ≈5–6 nm. MOP **5** can be fully loaded with doxorubicin (DOX) prodrug **2** via hetero–ternary complex formation to yield **7**. The MOPs exhibit excellent stability toward neutral to slightly acidic pH in 10 mM sodium phosphate buffer, mitigating the concern of disassembly during circulation. The results of MTS assays show that MOP **7** is 10-fold more cytotoxic toward HeLa cells than equimolar quantities of DOX prodrug **2**. The enhanced cytotoxicity can be traced to a combination of enhanced cellular uptake of **7** and DOX release as demonstrated by flow cytometry and confocal fluorescence microscopy. The confluence of properties imparted by the polycationic MOP architecture and plug-and-play CB[*n*] complexation provides a potent new platform for drug delivery application.

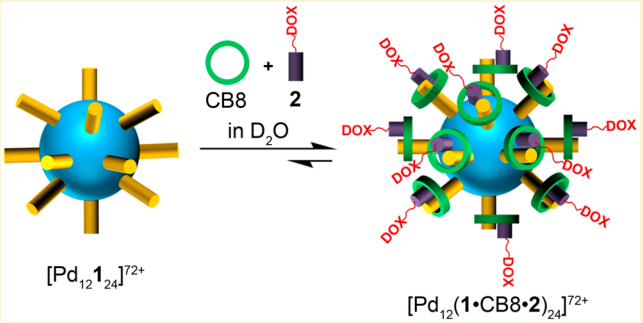

INTRODUCTION

A major thrust in chemistry, biology, and medicine in the past two decades has been the development of new drug delivery systems that improve drug efficacy and decrease side effects by controlling their pharmacokinetic and biodistribution profiles.[1,2] Accordingly, various drug delivery systems such as protein–drug conjugates, polymer–drug conjugates, polymersomes, nanomicelles, dendrimers, polymeric nanoparticles, and noble metal nanoparticles have been explored for cancer therapy and imaging.[3−5] Some of these drug delivery systems take advantage of the enhanced permeability and retention (EPR) effect, whereas others incorporate targeting ligands.[2,6] Despite these advances, the clinical application of some first-line chemotherapy drugs like doxorubicin (DOX) is limited by significant cardiotoxicity and rapid clearance.[7,8] One strategy to reduce toxicity toward normal cells is the development of prodrugs whose cytotoxicity is activated only in a tumor microenvironment (e.g., cathepsin B expression, acidic cytosol).[3,9] Unfortunately, some DOX prodrugs undergo sluggish cellular internalization that hampers their efficacy.[10] In this paper, we seek to combine the desirable structural properties of a nanoscale metal–organic polyhedron (MOP) scaffold with those of a DOX prodrug (**2**) self-assembled via host–guest assistance with cucurbit[8]uril.

In recent years, supramolecular chemists have used self-assembly processes to prepare functional self-assembled architectures of nanoscale dimensions driven by metal–ligand coordination interactions.[11−13] The integration of metal–ligand coordination assemblies with biological systems, particularly for drug delivery and diagnosis, is substantially less developed.[12,14−16] Previously, Stang, Chi, Therrien, and others have reported the anticancer activity of supramolecular coordination complexes.[17] The use of supramolecular coordination cages as anticancer drug delivery vehicles was first reported by Therrien.[15,18] Recently, Lippard reported a well-defined supramolecular system (a Pt(II) metallacycle) as a drug delivery vehicle to deliver a Pt(II) prodrug to cancer cells.[14] It is known that particle size influences the clearance rate of nanoparticles from the bloodstream, therefore compared to smaller sized coordination complexes studied previously (≤1.5 nm), we believe the larger sized supramolecular structures (≈5–6 nm) studied here should display slower renal clearance and longer circulation, which would be useful for theranostic applications and enhanced tumor uptake by the EPR effect.[5,8] Previously, the Fujita group has developed powerful strategies to synthesize large roughly spherical assemblies including cubooctahedral nanocages ($Pd_{12}L_{24}$ composition) by mixing Pd^{2+} and an angular bispyridine ligand (**L**).[19,20] An attractive aspect of this system is the capability of exohedral or endohedral cage functionalization via ligand (**L**) functionalization.[13] We envisioned that these large spherical assemblies,

Received: September 9, 2016
Published: October 10, 2016

DOI: 10.1021/jacs.6b09504
J. Am. Chem. Soc. 2016, 138, 14488–14496

when appropriately functionalized, would prove complementary to and thereby enrich the toolbox of nanoparticle-based drug delivery vehicles.[5,8,21−23]

Specifically, we sought to marry the geometrical features of metal−organic polyhedra (MOP) with the outstanding recognition properties of the cucurbit[*n*]uril family, which have unfolded rapidly over the past decade.[24−26] For example, CB[*n*] compounds exhibit ultratight binding affinity and high selectivity toward cationic guests in water and do so in a stimuli responsive (e.g., pH, chemical, photochemical, electrochemical) manner.[27,28] Furthermore, the elegant work of Kim, Scherman, and others show that larger CB[*n*] hosts (especially CB[8]) display the ability to form homo and hetero−ternary (e.g., host−guest−guest) complexes, whereby a cationic first guest (e.g., methyl viologen (**MV**), Chart 1) promotes the binding of

Chart 1. Chemical Structures of Compounds Used in This Study

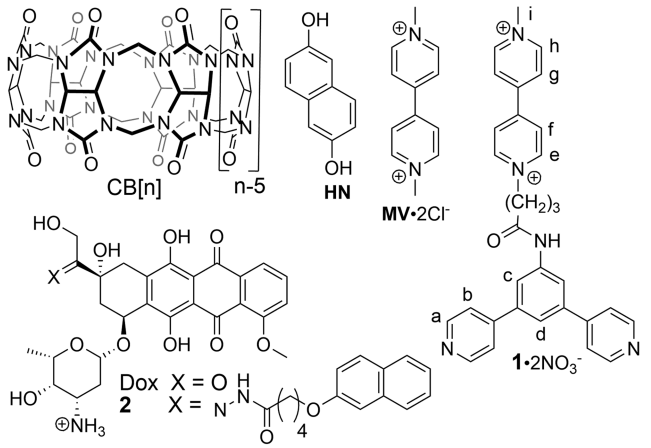

a neutral second guest.[26,27,29,30] These CB[8] controlled systems have been used to advantage in the preparation of supramolecular polymeric systems for biological and materials applications, chemical sensing ensembles, molecular machines, noncovalent promotors of biological dimerization, and supramolecular catalysis.[27,31,32] Given their excellent biocompatibility, other recent efforts have sought to use CB[*n*]-type receptors to enhance drug solubility, for imaging applications, and as a drug reversal agent.[31,33] Pioneering work in this area was performed by Yang, Zink, and Stoddart based on mesoporous silica nanoparticles that are gated by host·guest recognition processes.[23,34] In this paper, we decorate the external surface of Fujita-type $Pd_{12}L_{24}$ MOP with **MV** ligands, explore their noncovalent functionalization with CB[*n*], and demonstrate their ability to deliver DOX to cancer cells.

RESULTS AND DISCUSSION

Synthesis of Ligand (1) and Complexation with CB[*n*]. The synthesis of MOPs studded with MV units required the synthesis of ligand **1** (Scheme 1). First, methyl bipyridinium iodide was reacted with ethyl-4-bromobutyrate to afford compound **8**, which was hydrolyzed using aqueous HBr to give **9**. Suzuki coupling between 3,5-dibromoaniline and pyridine-4-boronic acid gave **10**. Carbodiimide-promoted amide-bond formation between **9** and **10** gave **1** in 78% yield. The spectroscopic characterization of all new compounds is given in the Supporting Information (SI).

Scheme 1. Synthesis of 1 and 2[a]

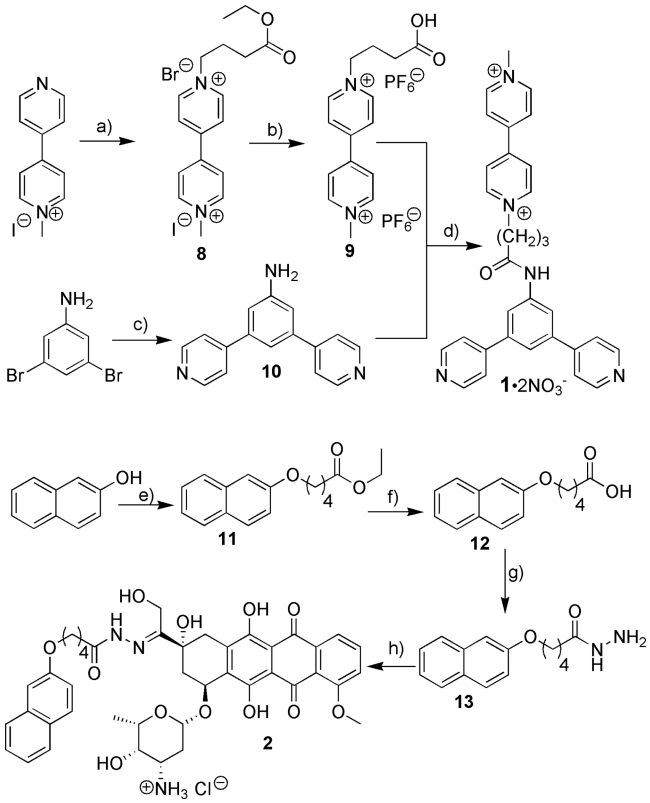

[a]Conditions: (a) ethyl-4-bromobutyrate, CH_3CN, 70 °C, 4 d, 40%; (b) 2 M HBr, H_2O, 2 d, NH_4PF_6, 80%; (c) $Pd(PPh_3)_4$, K_3PO_4, H_2O/1,4-dioxane (1:1), 80 °C, 4 d, 72%; (d) 1-ethyl-3-(3-dimethylaminopropyl)-carbodiimide, DMAP, DMF, 2 d, $(n\text{-}Bu)_4NNO_3$, CH_3CN, 30%; (e) Ethyl-5-bromovalerate, K_2CO_3, CH_3CN, 70 °C, 24 h, 82%; (f) LiOH, THF/H_2O (1:1), 70 °C, 24 h, 1 M HCl, 90%; (g) 1-ethyl-3-(3-dimethylaminopropyl)-carbodiimide, 1-hydroxybenzotriazole, CH_3CN, 3 h, N_2H_4 in CH_3CN 0−10 °C, 3 h, 65%; (h) Doxorubicin hydrochloride, trifluoroacetic acid, MeOH, 12 h, room temperature, 78%.

To determine whether CB[*n*] complexation with **1** might interfere with MOP formation or stability, we first studied the complexation with CB[7] and CB[8]. Diagnostic upfield shifting for H_f and H_g of ligand **1** when bound to CB[7] or CB[8] (SI, Figures S35 and S36) indicates that the **MV** subunit of **1** is the dominant binding site for CB[7] and CB[8].[25,35,36] CB[8]·**1** also maintains its ability to form the ternary charge-transfer complex CB[8]·**1**·**HN**, as evidenced by UV−vis spectroscopy and complexation-induced changes in chemical shift (SI, Figures S36 and S46).[35]

Synthesis and Characterization of MOP 3. Next, we synthesized MOP **3** = $[Pd_{12}\mathbf{1}_{24}](NO_3)_{72}$ by heating a mixture of **1** and $Pd(NO_3)_2{\cdot}2H_2O$ (0.5 equiv) at 60 °C in DMSO-d_6 for 24 h (Figure 1a). MOP **3** was characterized by ^{1}H NMR, diffusion-ordered spectroscopy (DOSY), and cold-spray ionization mass spectroscopy (CSI-MS). For example, the ^{1}H NMR spectra (Figure 1b,c) shows the typical downfield shifting of pyridine protons (H_a and H_b) upon formation of **3** (H_a: 8.69 to 9.42 ppm; H_b: 7.72 to 8.23 ppm).[19] The broadening of the bis(pyridine) resonances (H_a−H_d) reflect their slower tumbling motion with respect to the **MV** units of **3**. DOSY NMR (Figure 1d,e) was used to measure the diffusion coefficients for **3** (D = 3.55×10^{-11} m^2/s) and **1** (D = 3.20×10^{-10} m^2/s). The slower

DOI: 10.1021/jacs.6b09504
J. Am. Chem. Soc. 2016, 138, 14488−14496

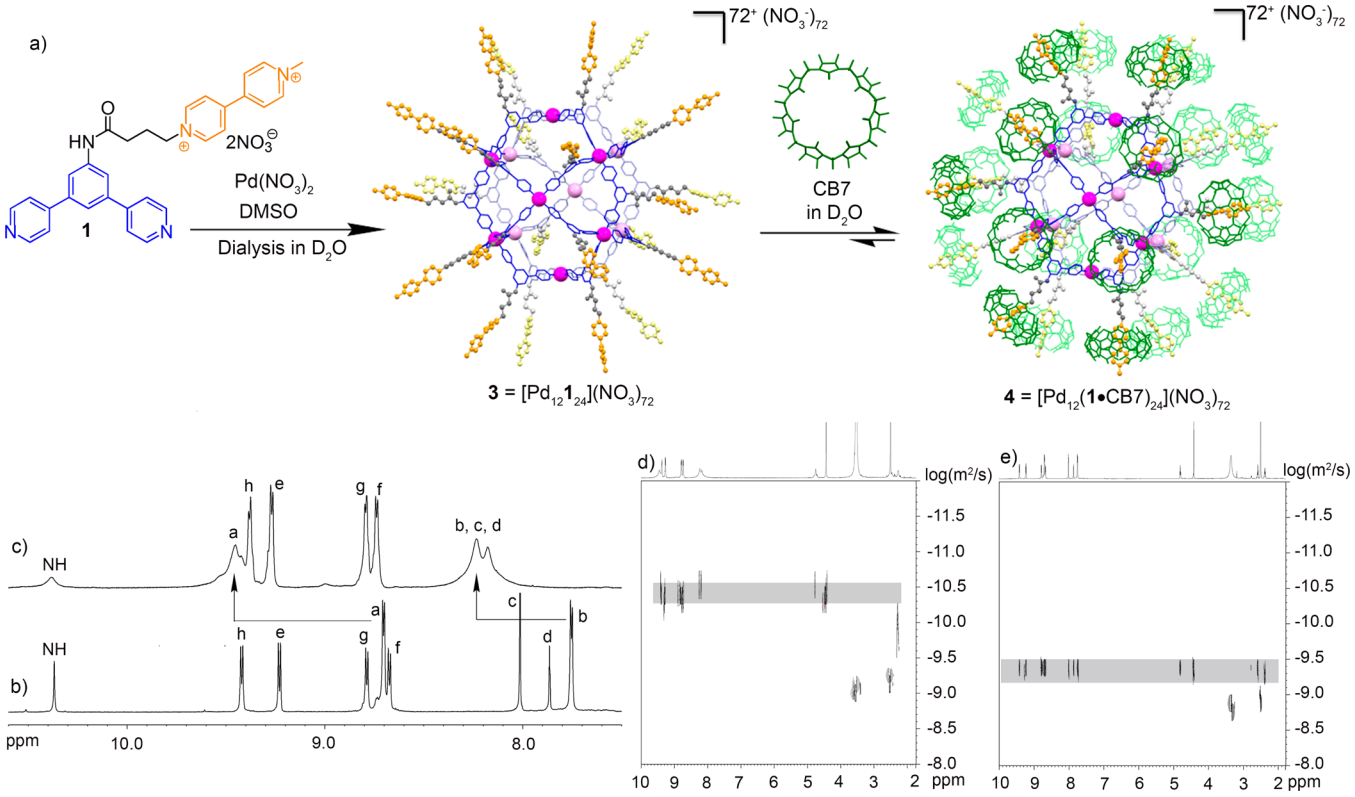

Figure 1. (a) Self-assembly of MOP **3** in DMSO and noncovalent capping with CB[7] to yield MOP **4** in D_2O. The depicted structures were rendered based on the MMFF minimized structures. ^{1}H NMR spectra recorded (600 MHz, DMSO-d_6, RT) for (b) **1** and (c) **3**. 2D ^{1}H DOSY NMR spectra recorded (600 MHz, DMSO-d_6, RT) for (d) **3** and (e) **1**.

diffusion of **3** reflects its larger diameter, which can be calculated using the Stokes−Einstein equation, as 6.2 nm, which agrees with the MMFF optimized structure of **3** (SI, Figure S61 and Table S1). CSI-MS provided further structural evidence of **3** following anion exchange from nitrate (NO_3^-) to triflate (OTf^-) via observation of a series of prominent ions $[M - x(OTf) + yDMSO]^{x+}$ (x = 15−40), which can be traced to the parent ion of **3** = $[Pd_{12}\mathbf{1}_{24}](OTf)_{72}$ (SI, Figure S23) with molecular weight of 17443.56 amu. MOP **3** is highly cationic (72+) due to its 12 Pd^{2+} ions and 24 pendant **MV** units which promote aqueous solubility. Accordingly, a DMSO-d_6 solution of **3** was dialyzed against D_2O (MWCO = 3500) for 24 h to afford an aqueous solution of **3**. MOP **3** can be isolated in solid form by removal of DMSO under high vacuum or by addition of EtOAc to the DMSO solution. The ^{1}H and DOSY spectra (SI, Figures S25 and S27) recorded for MOP **3** in D_2O are analogous to those measured in DMSO which establishes both the size (6.2 nm) and stability of **3** in water.

Capping of MOP 3 with CB[*n*]. After having firmly established the structure of **3**, we turned to an investigation of its supramolecular chemistry with CB[n] (n = 7, 8). Treatment of MOP **3** with CB[7] (24 equiv) in D_2O resulted in significant ^{1}H NMR upfield shifts for H_f and H_g (8.45 and 8.33 to 6.99 ppm) of the pendant **MV** units, which reflects their inclusion in the anisotropic shielding region of CB[7] (Figure 2a,b).[36] Figure 1a shows a molecular model of MOP **4** = $[Pd_{12}(\mathbf{1}\cdot CB7)_{24}](NO_3)_{72}$. The DOSY NMR for **4** (Figure 2e) clearly shows a single band at $D = 9.55 \times 10^{-11}$ m^2/s; in contrast free CB[7] diffuses much faster ($D = 5.0 \times 10^{-10}$ m^2/s, SI, Figure S30), which indicates that the CB[7] molecules are bound to the **MV** units studding the nanosphere. The UV−vis titration of

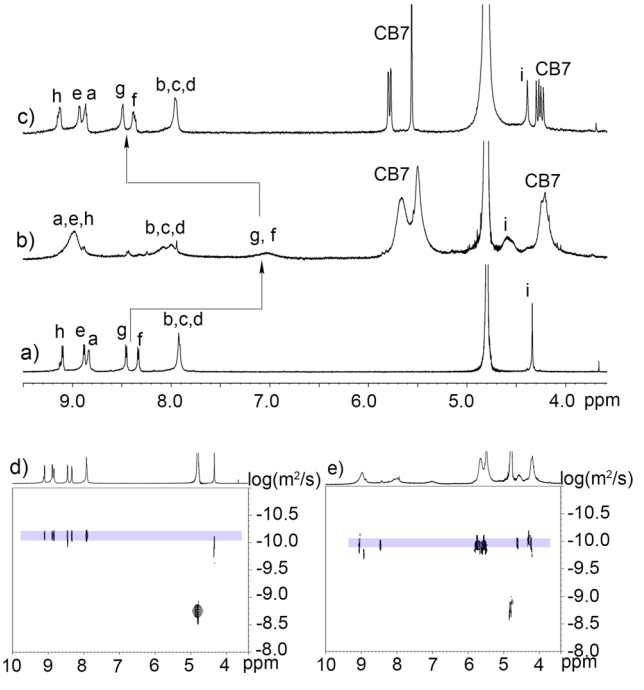

Figure 2. ^{1}H NMR spectra recorded (600 MHz, D2O, RT) for (a) **3**, (b) **4**, and (c) **4** with 24 equiv of ADA. 2D ^{1}H DOSY NMR spectra recorded (600 MHz, D2O, RT) for (d) **3** and (e) **4**.

3 (2.0 μM) with CB7 (0−30 μM) shows a decrease in absorbance at 274 nm, which is diagnostic for CB7·**MV** complexation (SI, Figure S45). The plot of absorbance versus CB[7] concentration could be fitted to a 1:1 binding model (K_a

DOI: 10.1021/jacs.6b09504
J. Am. Chem. Soc. 2016, 138, 14488−14496

= (1.6 ± 0.7) × 10^6 M^{-1}), assuming all 24 binding events are independent. The plot shows a plateau at a MOP **3**:CB[7] stoichiometry of 1:24 which allowed us to calculate that >90% of CB[7] is bound to MOP **3** under these conditions. Remarkably, a comparison of the DOSY spectra of **3** and **4** (Figure 2d,e) indicates that the complexation of 24 MV units by CB[7] does not increase the hydrodynamic diameter of MOP **4** (5.2 nm) even though molecular weight increases by 27911 amu! In contrast, the diameter of MOP **4** (d = 5.2 nm) decreases by ≈1.0 nm compared to MOP **3** (d = 6.2 nm) as evidenced by DOSY NMR (SI, Table S1). We attribute this smaller diameter to hydrophobic interactions between the outer surface of CB7 and the aromatic scaffold of the MOP.

Despite numerous attempts, we were unable to grow single crystals of sphere **4**. However, we were successful in visualizing MOP **4** by transmission electron microscopy (TEM), which revealed both the size (4−5 nm diameter) and spherical shape of individual MOPs upon deposition of aqueous solution of **4** on carbon-coated Cu grids (SI, Figure S55). Furthermore, we obtained atomic force microscopy (AFM) images of **4** deposited on a freshly cleaved mica surface, which showed particles with a height of 5−6 nm above the surface, consistent with the anticipated diameter (SI, Figure S59). The noncovalent CB[7] caps on the **MV** studded surface of **4** can be reversed in a stimuli responsive fashion[26,27] by the addition of adamantane ammonium (**ADA**) to regenerate **3** along with the ultratight CB[7]·**ADA** complex (Figure 2c).

In a similar manner, we capped the MV studs of **3** with CB[8] to afford MOP **5** = $[Pd_{12}(\mathbf{1}\cdot CB8)_{24}](NO_3)_{72}$ (Figure 3a). As expected, the H_f and H_g protons exhibit an upfield shift ($\Delta\delta \approx 0.7$ ppm) upon complexation with CB[8] (Figure 3b,c) ,whereas H_i, which is located near the deshielding ureidyl C═O portals, moves slightly downfield. DOSY NMR establishes that the MOP and CB[8] units in **5** diffuse at the same rate (D = 8.91 × 10^{-11} m^2/s), which is much slower than free CB[8] (D = 3.16 × 10^{-10} m^2/s, SI Figure S34), indicating that the CB[8] molecules are noncovalently attached to nanosphere **3**. We visualized **5** by both TEM and AFM microscopy. TEM images (Figure 4a) show the spherical shape of the particles with an average diameter of 5.2 nm (SI, Figure S56). The particle height observed by AFM images of **5** (≈5.5 nm, Figure 4b) is consistent with the MMFF minimized diameter of **5** (SI, Figure S63).

Hetero Ternary Complexation with MOP 5. Given the ability of CB8·**MV** to form hetero−ternary complexes with various second guest molecules,[26,27,29,35] we envisioned that **5** would be useful for the complexation of payloads on its CB[8] studded surface. As proof-of-principle, we choose the well-known second guest 2,6-dihydroxynaphthalene (**HN**). Accordingly, we monitored the addition of **HN** (24 equiv) to an aqueous solution of **5** by both ^{1}H NMR and UV−vis spectroscopy (Figure 3d and 4c) which yields MOP **6** = $[Pd_{12}(\mathbf{1}\cdot CB8\cdot \mathbf{HN})_{24}](NO_3)_{72}$ (Figure 3a). As expected based on literature precedent, protons H_f and H_g of **MV** unit and the **HN** protons undergo further upfield shifting (to 6.94 and 6.74 ppm) upon hetero−ternary complex formation of MOP **6**.[35] The formation of **6** is based on charge-transfer interactions, and accordingly, UV−vis titration of **5** (20 μM) with **HN** (0−500 μM) displays a long wavelength absorbance at 570 nm that is diagnostic for the heteroternary complexation (Figure 4c).

Design, Synthesis, and pH-Responsive Behavior of Prodrug 2. The ability of MOP **5** to form hetero−ternary complexes suggested its use as a scaffold for the delivery of

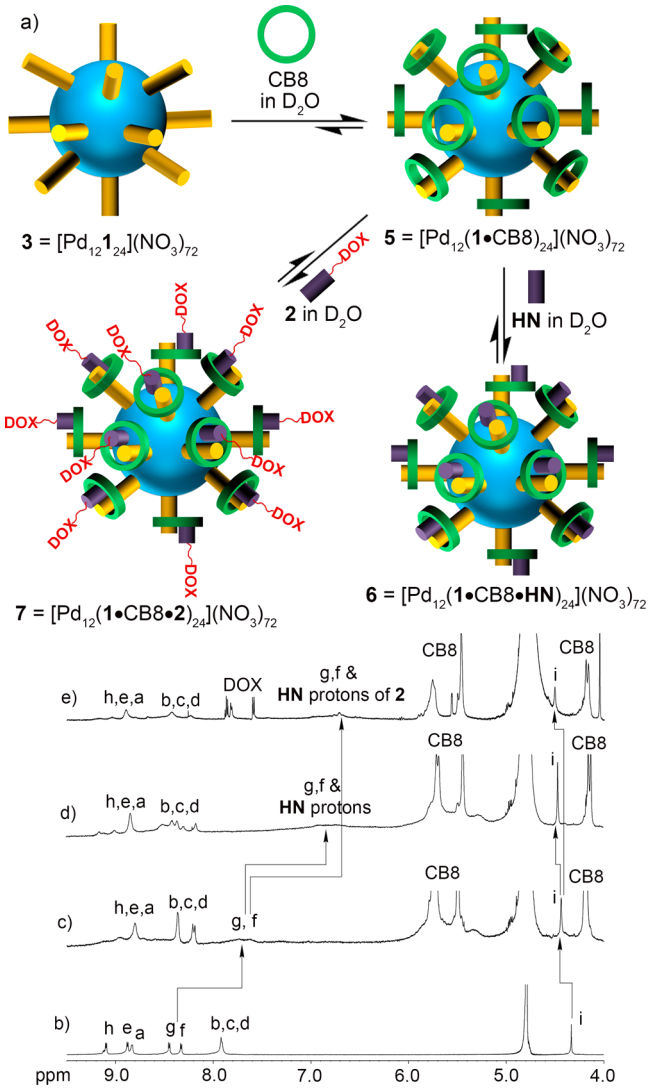

Figure 3. (a) Sequential self-assembly of the **MV** units of MOP **3** as first guest with CB[8] to yield MOP **5** followed by hetero−ternary complex formation with **HN** or **2** to yield MOP **6** and MOP **7**. ^{1}H NMR recorded (600 MHz, D_2O, RT) for (b) **3**, (c) **5**, (d) **6**, and (e) **7**.

anticancer drugs. We expected that both the size and high charge of **5** would influence the cellular uptake and trafficking *in vitro* and perhaps exhibit the EPR effect when used *in vivo* and show enhanced biodistribution and pharmacokinetics.[14,37] For this purpose, we initially explored the complexation of the potent anticancer drug DOX with **5** but did not observe ternary complex formation by ^{1}H NMR spectroscopy (SI, Figure S38). As an alternative to a direct complexation strategy, we designed DOX prodrug **2** which features a 2-alkoxynaphthalene substituent covalently connected to DOX. Such 2-alkoxynaphthalenes are known to form strong ternary complexes (K_a = 10^5 M^{-1}) with CB[8]·**MV**.[29] Accordingly, we synthesized **2** in four steps, as shown in Scheme 1. First, 2-hydroxynaphthalene was reacted with ethyl-5-bromovalerate to give **11**, which was hydrolyzed by LiOH to give **12**. Next, carboxylic acid **12** was transformed into acyl hydrazine **13**. Lastly, **13** and DOX were reacted to give acyl hydrazone DOX prodrug **2**.

To minimize side effects and exhibit maximum therapeutic efficacy, it is imperative that **2** releases DOX after internalization by cancer cells. The design of **2** capitalized on the more

DOI: 10.1021/jacs.6b09504
J. Am. Chem. Soc. 2016, 138, 14488−14496

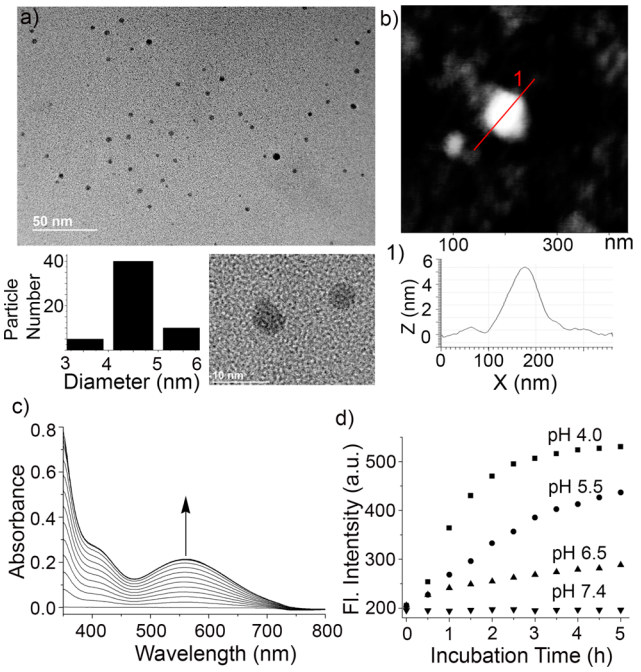

Figure 4. (a) TEM image of **5** and the statistical distribution of particle size of **5**. (b) AFM image of **5** and its height profile. (c) UV−vis titration of **5** (20 μM) with **HN** (0−500 μM) in water. (d) Plot of change in fluorescence intensity at λ_{max} = 597 nm versus time after incubating **2** in buffer at pH 7.4, 6.5, 5.5, and 4.0.

acidic environment of cancer cells and the acid labile nature of the hydrazone bond of **2**. The UV−vis spectrum of **2** is quite similar to free DOX, but the fluorescence emission of **2** is reduced 2.6-fold relative to DOX (SI, Figures S47 and S48).[38] To test the pH responsiveness, **2** (20 μM) was incubated in 10 mM sodium phosphate buffer at pH 7.4 and 10 mM sodium acetate buffer at pH 6.5, 5.5, and 4.0, and the fluorescence emission spectra was measured for 5 h (SI, Figures S51−S54). Figure 4d shows a plot of fluorescence emission intensity at 597 nm as a function of incubation time and pH. At pH 7.4, no release of DOX was observed after 5 h, whereas 55% and 80% of DOX were released at pH 6.5 and 5.5, respectively. At pH 4.0, >90% of DOX was released from **2** within 3 h, establishing the pH responsiveness of **2** at endo- and lysosomal pH of cancer cells. In this manner, **2** is expected to deter release of DOX during circulation and promote its release only after cellular uptake, which should enhance its efficacy.

Loading MOP 5 with Prodrug 2. Next, we decided to load MOP **5** with DOX as cargo in the form of prodrug **2** (inherent D_2O solubility (830 μM). Accordingly, **5** was treated with 24 equiv of **2** in D_2O to give MOP **7** = $[Pd_{12}(\mathbf{1}\cdot CB8\cdot \mathbf{2})_{24}](NO_3)_{72}$. ^{1}H NMR shows that the naphthalene protons of **2** undergo upfield shift (Figure 3e) to 6.72 ppm (similar to that observed for [CB8·**MV**·**2**], SI, Figure S39), which reflects the binding of **2** to **5** based on CB8·**MV**·**HN** type hetero−ternary complexation as shown in Figure 3a. The presence of a strong UV−vis absorbance for **2** at 500 nm complicates monitoring of the appearance of the charge-transfer band for **7**. However, quenching of fluorescence emission (λ_{max} = 370 nm) of the naphthalene unit of **2** within assembly **7** confirms the formation heteroternary complex (SI, Figure S50).[35] Importantly, DOSY NMR (SI, Figure S41) shows that MOP **7** diffuses at same rate (D = 6.31 × 10^{-11} m^2/s) observed for **5**. Moreover, we visualized MOP **7** by TEM, which revealed both the size and spherical shape of MOPs upon deposition on carbon coated Cu grids. The particle size was measured to be 5.4 nm (SI, Figure S57).

As a control experiment, we tested the ability of uncapped MOP **3** to bind DOX and its prodrug **2** within the cuboctahedral cavity. DOSY NMR (SI, Figures S43 and S44) of equimolar mixture of MOP **3** and DOX or MOP **3** and **2** establish that both DOX (D = 3.55 × 10^{-10} m^2/s) and **2** (D = 3.16 × 10^{-10} m^2/s) diffuse at much faster rate compared to MOP **3** (D = 6.3 × 10^{-11} m^2/s). Accordingly, we conclude that neither DOX nor prodrug **2** undergo complexation inside the large cubooctahedral cavity of MOP **3**. The combined inference of all these experiments supports the depicted structure of **7** promoted by heteroternary complex formation and further validates the potential of **5** as a new drug delivery vehicle.

Stability and Surface Charge of MOPs. The use of the MOPs in therapeutic or diagnostic applications requires high stability under mildly acidic conditions. Accordingly, we verified the stability of MOP **5** from neutral to slightly acidic pH by TEM and AFM images. Figure 5c shows a TEM image of MOP

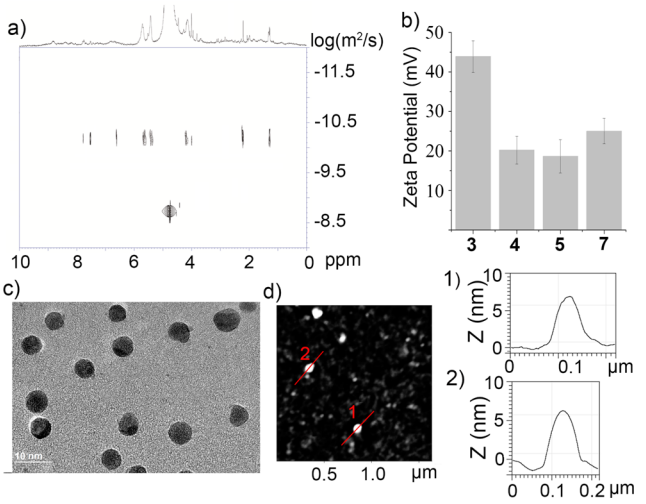

Figure 5. (a) DOSY NMR of MOP **7** in sodium phosphate buffer (10 mM) at pH 7.4. (b) Zeta potential of MOP **3**, MOP **4**, MOP **5**, and MOP **7**. (c) TEM image of MOP **5** at pH 5.5. (c) AFM image of MOP **5** at pH 5.5 and its height profile (1 and 2).

5 at pH 5.5 that shows particles of 5.6 nm diameter, which is similar to that observed at neutral pH (*vide supra*). Similarly, an AFM image (Figure 5d) of MOP **5** at pH 5.5 shows particles of 5.8 nm height. We also established the stability of MOP **7** in 10 mM sodium phosphate buffer at pH 7.4 by ^{1}H and DOSY NMR (D = 5.62 × 10^{-11} m^2/s, Figure 5a). During *in vivo* studies, MOPs will encounter acidic pH environment only after reaching the tumor site. The excellent stability of MOPs at neutral to slightly acidic pH and in biologically meaningful sodium phosphate buffer (10 mM, pH 7.4) strongly suggests MOPs disintegration during systemic circulation will not occur.

In addition to nanoparticle size, the surface chemistry of nanoparticles plays important role in influencing cellular uptake,[39] the composition of protein "corona" developing around NPs *in vivo*,[40] and their suborgan distributions.[22] Decreased size and reduced zeta potential (ζ) increases the circulation time by reducing the interaction with host cells.[41] MOP **3** is found to be highly cationic (ζ = +43 mV). However, upon complexation of the **MV** studs of MOP **3** by CB[7] or

DOI: 10.1021/jacs.6b09504
J. Am. Chem. Soc. 2016, 138, 14488−14496

CB[8] (e.g., **4** and **5**), the ζ potential decreases significantly. The surface potential (ζ) of MOP **4** and MOP **5** was measured to be +20.2 mV and +18.6 mV (Figure 5b). We attribute this decrease in ζ potential to the shielding of the surface charge by electronegative ureidyl C═O portals of CB[*n*]. The zeta potential of drug loaded MOP **7** was determined to be 25.0 mV, which is slightly larger than MOP **5** presumably due to the presence of cationic prodrug **2**. The excellent stability, nanoscale size, and reduced zeta potential of the CB[*n*] capped MOPs make them an attractive new candidate for drug delivery applications.

***In vitro* Cytotoxicity.** A comparative investigation of free **2** versus **2** formulated as part of nanosphere **7** allowed us to assess the influence of the nanosphere on cellular uptake and cytotoxicity. First we incubated **2** or **7** with human cervical cancer cells (HeLa) for 1 h up to 12 h. Cellular uptake was then measured using flow cytometry (Figure 6a). The mean

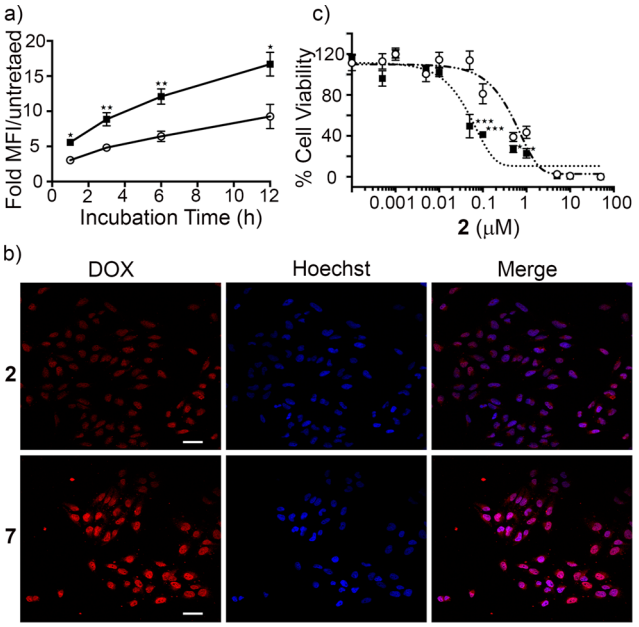

Figure 6. (a) Plot of normalized MFI versus incubation time derived from flow cytometry experiments (N = 4) for HeLa cells treated with **2** (1 μM, ○) or **7** ([**2**] = 1 μM, ■) for 1, 3, 6, or 12 h. (b) Confocal fluorescence microscopy of HeLa cells treated with **2** (5 μM) or **7** ([**2**] = 5 μM) at 40× magnification. Scale bar = 30 μm. (c) Results of MTS assay for HeLa cells treated with **2** (○) or **7** (■). Curve fitting of cytotoxicity data for **2** (–···–) and **7** (···) yielded EC_{50} values of 500 ± 110 nM and 48 ± 8 nM, respectively (N = 15). *p < 0.05, **p < 0.01, ***p < 0.001.

fluorescence intensity (MFI) of HeLa cells treated with **2** (1 μM) increases from 3.0- to 9.3-fold dependent on incubation time compared to untreated cells. Under the same conditions, the MFI of cells treated with **7** ([**2**] = 1 μM) increases from 5.6- to 16.7-fold compared to untreated cells. Subsequently, the cellular location of drug was evaluated by confocal fluorescence microscopy (Figure 6b). HeLa cells were incubated with **2** or **7** for 1 h. Confocal fluorescence microscopy images demonstrated red fluorescence of DOX in the nucleus, as confirmed by colocalization with the blue fluorescence from the nuclear stain Hoechst 33342. We used the Hoechst 33342 nuclear fluorescence intensity as a reference to quantify nuclear DOX. The ratio of red to blue fluorescence intensity was measured for 15 nuclei per image, and mean ± SEM was calculated as 0.529 ± 0.03 and 1.113 ± 0.100 for **2** and **7**, respectively (***p < 0.001, SI, Figure S66). This 2-fold higher drug concentration in the nuclei for **7** compared to free **2** is in agreement with the 2-fold better uptake of **7** than free **2** measured by flow cytometry.

Finally, we evaluated the cytotoxicity of **2** and **7** (Figure 6c). We incubated HeLa cells with **7** and separately with **2** for 72 h. MTS assays were performed to measure cell viability. Nanosphere **7** displays significantly higher potency (IC_{50} = 48 ± 8 nM) against HeLa cells compared to free prodrug **2** (IC_{50} = 500 ± 110 nM). In fact, the cytotoxicity of **7** is comparable to free DOX (IC_{50} = 34 ± 11 nM, SI, Figure S65) but should display *in vivo* characteristics due to longer circulation time and better tumor uptake via the EPR effect. Importantly, delivery vehicle alone (MOP **5**) shows no toxicity against HeLa cells at these concentrations (SI, Figure S64). We conclude that 10-fold higher cytotoxicity of **7** toward HeLa cells is due to a combination of better cellular uptake of **7** and pH triggered DOX release from prodrug **2** inside HeLa cancer cells.

CONCLUSION

In summary, we have reported the design, synthesis, and evaluation of MOP **3** as a prodrug delivery vehicle. MOP **3** is studded with 24 **MV** units, which enables it to undergo well-defined 1:1 host–guest interactions with CB[7] and CB[8]. Advantageously, MOP **5** can be loaded with up to 24 molecules of DOX prodrug **2** by CB[8] promoted hetero–ternary charge-transfer complex formation. The release of free DOX from **7** occurs by cleavage of the acid sensitive acylhydrazone linkage. MOP **7** is taken up better by HeLa cells than free **2**, which results in a 10-fold decrease in the IC_{50} value to 48 nM. Importantly, the cytotoxicity of MOP **7** (IC_{50} = 48 nM) is comparable to free DOX (IC_{50} = 34 nM), which shows that the nanoscale architecture of **7** imparts improved properties (e.g., uptake) but does not diminish the inherent activity of the drug. Looking forward, we expect that the larger nanoscale architecture of MOP **7** (≈ 5–6 nm) and related constructs should benefit from longer circulation times *in vivo* and potentially reduce side effects due to preferential accumulation in tumors due to the EPR effect. Due to large size and excellent stability in phosphate buffer and slightly acidic to neutral pH, we believe that the merger between functionalized MOP and the recognition properties of CB[*n*] molecular containers enables a wide range of applications by virtue of the plug-and-play nature of the CB[8]-induced hetero–ternary complexation. For example, plugging with a multiplicity of prodrugs, fluorophores, PET imaging agents, and targeting ligands is readily envisaged and will enable (multiply) targeted drug delivery, fluorescence, or PET imaging for diagnostic and theranostic applications with great potential to improve human health.[5,8]

EXPERIMENTAL SECTION

General. Starting materials were purchased from commercial suppliers and were used without further purification. Melting points were measured on a Meltemp apparatus in open capillary tubes and are uncorrected. IR spectra were measured on a Thermo Nicolet NEXUS 670 FT/IR spectrometer by attenuated total reflectance (ATR) and are reported in cm^{-1}. NMR spectra were measured at 400, 500, or 600 MHz for ^{1}H and 100 and 125 MHz for ^{13}C using deuterated water (D_2O), deuterated chloroform ($CDCl_3$), or deuterated dimethyl sulfoxide (DMSO-d_6) as solvent. Chemical shifts (δ) are referenced relative to the residual resonances for HOD (4.79 ppm), $CHCl_3$ (7.26 ppm for ^{1}H, 77.16 ppm for ^{13}C), and DMSO-d_6 (2.50 ppm for ^{1}H, 39.51 ppm for ^{13}C). Mass spectrometry was

DOI: 10.1021/jacs.6b09504
J. Am. Chem. Soc. 2016, 138, 14488–14496

performed using a JEOL AccuTOF electrospray instrument for routine sample. CSI-MS was performed using Bruker 12T Apex IV FT-ICR-MS at the University of Maryland, Baltimore County. TEM was performed on a JEOL JEM 2100. A Digital instruments nanoscope III multimode AFM was used for surface characterization. Molecular modeling (MMFF) was performed using Spartan '08 on a personal computer.

Compound [1·2NO$_3$]. Compound **9** (350 mg, 0.638 mmol) and **10** (157 mg, 0.638 mmol) were dissolved in DMF (15 mL) completely. Then, 1-ethyl-3-(3-(dimethylamino)propyl)carbodiimide (365 mg, 1.91 mmol) and *N*,*N*-dimethylaminopyridine (77.6 mg, 0.635 mmol) were added to the solution sequentially and stirred at RT for 48 h under N_2. DMF was removed completely under reduced pressure, and then diethyl ether (15 mL) was added to the crude solid and sonicated for 10 min. The mixture was centrifuged to collect the solid material. The crude solid was then washed with chloroform (3 × 15 mL) by sonication, and solid was collected by centrifugation. Then solid was washed with hot water (3 × 15 mL) using sonication, and solid material was collected by centrifugation to afford compound [**1**·2PF$_6$] as a brown solid. The solid was then dried under high vacuum. Then solid material was dissolved completely in acetonitrile (5 mL). Then a concentrated solution of $(n\text{-Bu})_4NO_3$ (1.0 g in 1 mL of acetonitrile) was added to the solution leading to precipitation. The solid was collected by centrifugation and further washed with acetonitrile (3 × 5 mL) by sonication. Finally the solid was collected by centrifugation and dried under high vacuum to afford compound [**1**·2NO$_3$] as a gray white solid (90 mg, 30%). Mp 250−251 °C, IR (ATR, cm^{-1}) 2920m, 2850w, 1690s, 1593s, 1546s, 1443m, 1429m, 1407s, 1284w, 1221w, 1141w, 1114s, 1070w, 1029w, 994m, 960w, 885m, 814s. 1H NMR (600 MHz, DMSO-d_6): δ = 10.35 (s, 1H), 9.42 (d, J = 6.6 Hz, 2H), 9.23 (d, J = 6.6 Hz, 2H), 8.79 (d, J = 6.6 Hz, 2H), 8.69 (d, J = 6.6 Hz, 4H), 8.67 (d, J = 6.6 Hz, 2H), 7.99 (d, J = 1.2 Hz, 2H), 7.85 (s, 1H), 7.72 (d, J = 6.6 Hz, 4H), 4.80 (t, J = 6.9 Hz, 2H), 4.41 (s, 3H), 2.58 (t, J = 6.9 Hz, 2H), 2.38 (m, J = 7.2 Hz, 2H). ^{13}C NMR (150 MHz, DMSO-d_6): δ = 173.4, 160.5, 150.2, 148.7, 148.2, 146.6, 146.5, 145.9, 139.6, 126.5, 126.0, 121.6, 117.8, 113.2, 60.3, 48.0, 30.2, 26.0. MS (ESI, positive) m/z 242 (100%, [M−2NO$_3$]$^{2+}$).

Compound 2. Compound **13** (27.0 mg, 103 μmol) and DOX hydrochloride (20.0 mg, 34.5 μmol) were dissolved in dry MeOH (8 mL) under N_2. Then trifluoroacetic acid (40 μL) was added to catalyze the reaction, which was protected from light with aluminum foil and stirred for 12 h. Then, the solution was concentrated to a volume of ∼1 mL by rotary evaporation. Dry EtOAc (2 mL) was added to the solution and sonicated for 5 min. A dark red precipitate was observed. The precipitate was collected by centrifugation. The solid was dried under high vacuum to give **2** as a dark red solid (22 mg, 78%). Mp 119−120 °C, IR (ATR, cm^{-1}) 3190w, 3020w, 2840w, 2638w, 1690s, 1629m, 1600s, 1581m, 1467s, 1389s, 1259s, 1216s, 1180s, 1169s, 1117m, 1029s, 1018s, 985s, 913w, 840s, 814s, 763w, 743s. ^{1}H NMR (600 MHz, DMSO-d_6) δ = 10.37 (s, 1H), 7.90−7.84 (m, 2H), 7.76 (brs, 3H), 7.72−7.67 (m, 3H), 7.55 (d, J = 8.4 Hz, 1H), 7.34 (t, J = 7.5 Hz, 1H), 7.23 (t, J = 7.5 Hz, 1H), 7.08 (d, J = 2.4 Hz, 1H), 6.97 (dd, J = 9.0 Hz, J = 2.4 Hz, 1H), 5.76 (brs, 1H), 5.44 (brs, 1H), 5.41 (s, 1H), 5.31 (d, J = 3.0 Hz, 1H), 4.94 (t, J = 6.6 Hz, 1H), 4.43 (m, 2H), 4.06−3.99 (m, 2H), 3.90 (s, 3H), 3.88 (t, J = 6.0 Hz, 2H), 3.54 (s, 1H), 3.28 (d, J = 17.4 Hz, 1H), 2.76 (d, J = 17.4 Hz, 1H), 2.46−2.43 (m, 2H), 2.38−2.32 (m, 3H), 2.17 (dd, J = 13.5 Hz, J = 6.3 hz, 1H), 1.88 (td, J = 12.6 Hz, J = 3.6 Hz, 1H), 1.71 (dd, J = 12.3 Hz, J = 3.0 Hz, 1H), 1.59−1.54 (m, 4H), 4.18−4.16 (m, 4H). ^{13}C NMR (150 MHz, DMSO-d_6) δ = 187.0, 186.9, 171.9, 161.3, 157.0, 156.5, 154.9, 136.7, 135.7, 135.2, 134.8, 134.6, 129.7, 128.9, 127.9, 127.1, 126.8, 123.9, 120.4, 120.2, 119.5, 119.2, 111.2, 111.1, 107.1, 99.7, 75.2, 70.2, 67.6, 66.6, 66.6, 64.2, 57.1, 47.0, 36.8, 33.5, 32.5, 28.7, 22.4, 19.0, 17.2. HR-MS: m/z 784.3074 ([M]$^+$, calcd for [C$_{42}$H$_{46}$N$_3$O$_{12}$]$^+$, 784.3081).

3 = [Pd$_{12}$1$_{24}$](NO$_3$)$_{72}$. **1** (5.50 mg, 8.99 μmol) was taken in a 2 dram vial, and Pd(NO$_3$)$_2$·2H$_2$O (1.20 mg, 4.49 μmol) dissolved in DMSO-d_6 (250 μL) was added. Additional 250 μL of DMSO-d_6 was added to the mixture. The reaction mixture was stirred at 60 °C for 24 h to afford the [Pd$_{12}$**1**$_{24}$](NO$_3$)$_{72}$ quantitatively as a dark brown solution. [Pd$_{12}$**1**$_{24}$](NO$_3$)$_{72}$ was characterized by ^{1}H NMR, ^{13}CNMR, CSI-MS, and DOSY. Then solution of [Pd$_{12}$**1**$_{24}$](NO$_3$)$_{72}$ was transferred to a dialysis tube (MWCO 3500) and dialyzed the solution for 24 h against D_2O (every 3 h D_2O was replaced fresh D_2O). Mp 207−208 °C, IR (ATR, cm^{-1}) 2962w, 1757s, 1730s, 1640w, 1615w, 1510w, 1391m, 1336m, 1245m, 1222w, 1213w, 1183m, 1025m, 1006m, 831m, 760w. ^{1}H NMR (600 MHz, DMSO-d_6) δ = 10.38 (s, 24H), 9.42 (brs, 96H), 9.38 (s, 48H), 9.28 (d, J = 6.6 Hz, 96H), 8.79 (s, 48H), 8.75 (d, J = 6.6 Hz, 48H), 8.23 (brs, 168H), 4.75 (brs, 48H), 4.43 (s, 72H), 2.78 (s, 48H), 2.27 (s, 48H). ^{13}C NMR (150 MHz, DMSO-d_6) δ = 173.4, 160.7, 151.0, 149.2, 148.7, 148.2, 146.7, 145.9, 136.4, 126.5, 126.1, 124.4, 118.3, 114.9, 60.3, 48.0, 30.2, 26.7 ppm. [Pd$_{12}$**1**$_{24}$](NO$_3$)$_{72}$ was treated with excess NaOTf (100 equiv) in water to afford [Pd$_{12}$**1**$_{24}$](OTf)$_{72}$ and subjected to mass instrument. CSI-Ms (m/z): 1483.5 [Pd$_{12}$**1**$_{24}$](OTf)$_{57}$ + 10DMSO]$^{15+}$, 1396.5 [Pd$_{12}$**1**$_{24}$](OTf)$_{56}$ + 13DMSO]$^{16+}$, 1311.6 [Pd$_{12}$**1**$_{24}$](OTf)$_{55}$ + 14DMSO]$^{17+}$, 1224.6 [Pd$_{12}$**1**$_{24}$](OTf)$_{54}$ + 13DMSO]$^{18+}$, 1139.6 [Pd$_{12}$**1**$_{24}$](OTf)$_{53}$ + 10DMSO]$^{19+}$, 1052.6 [Pd$_{12}$**1**$_{24}$](OTf)$_{52}$ + 4DMSO]$^{20+}$, 1025.6 [Pd$_{12}$**1**$_{24}$](OTf)$_{51}$ + 12DMSO]$^{21+}$, 967.6 [Pd$_{12}$**1**$_{24}$](OTf)$_{50}$ + 11DMSO]$^{22+}$, 938.6 [Pd$_{12}$**1**$_{24}$](OTf)$_{49}$ + 17DMSO]$^{23+}$, 880.7 [Pd$_{12}$**1**$_{24}$](OTf)$_{48}$ + 13DMSO]$^{24+}$, 852.7 [Pd$_{12}$**1**$_{24}$](OTf)$_{47}$ + 17DMSO]$^{25+}$, 795.7 [Pd$_{12}$**1**$_{24}$](OTf)$_{46}$ + 11DMSO]$^{26+}$, 708.8 [Pd$_{12}$**1**$_{24}$](OTf)$_{44}$ + 4DMSO]$^{28+}$, 681.7 [Pd$_{12}$**1**$_{24}$]-(OTf)$_{42}$ + 15DMSO]$^{30+}$, 633.5 [Pd$_{12}$**1**$_{24}$](OTf)$_{40}$ + 17DMSO]$^{32+}$, 580.0 [Pd$_{12}$**1**$_{24}$](OTf)$_{38}$ + 14DMSO]$^{34+}$, 538.8 [Pd$_{12}$**1**$_{24}$](OTf)$_{46}$ + 14DMSO]$^{36+}$, 509.8 [Pd$_{12}$**1**$_{24}$](OTf)$_{34}$ + 17DMSO]$^{38+}$, 450.9 [Pd$_{12}$**1**$_{24}$](OTf)$_{32}$ + 4DMSO]$^{40+}$.

Cell Culture. HeLa cells were grown in Dulbecco's Modified Eagle Medium (DMEM, Gibco Corp) with 10% feral calf serum (FCS, ATLANTA biologicals) and 1% penicillin/streptomycin (Pen/Strep, Gibco Corp) at 37 °C and 5% CO_2.

Uptake of 2 and 7 = [Pd$_{12}$(1·CB8·2)$_{24}$](NO$_3$)$_{72}$. The efficiency of drug delivery of **5** = [Pd$_{12}$(**1**·CB8)$_{24}$](NO$_3$)$_{72}$ was evaluated by flow cytometry. HeLa cells were plated at 2 × 10^5 cells/well in 24 wells plate overnight (TPP, Switzerland). Cells were then incubated for 1, 3, 6, or 12 h with 1 μM of **2** or **7**. Untreated cells were used as control. Cells were detached and washed three times with Dulbecco's Phosphate Buffer Saline (DPBS, Gibco Corp). Red fluorescence was analyzed using a 585/42 emission filter of a Canto II flow cytometer (BD bioscience). Results were expressed as the fold of the MFI obtained versus those of untreated cells (eq 1):

$$\text{fold MFI untreated} = \text{MFI}_{\text{sample}}/\text{MFI}_{\text{untreated}} \quad (1)$$

Cytotoxicity of 2 and 7 = [Pd$_{12}$(1·CB8·2)$_{24}$](NO$_3$)$_{72}$. The cytotoxicity of **2** and **7** were evaluated using CellTiter 96 aqueous nonradioactive cell proliferation assay (Promega Corporation). First, 5 × 10^3 HeLa cells/well were plated overnight in a 96 well plate (Corning). Then cells were incubated for 72 h with a concentration range of **2** or **7** from 0.0001 μM to 50 μM. Cells were washed 3 times with DPBS, and then MTS solution was added for 1 h. Absorbance at 490 nm was measured. Percentage of viable cells was calculated using an untreated group as control using eq 2:

$$\text{cell viability}(\%) = (\text{ABS}_{\text{sample}}/\text{ABS}_{\text{untreated}}) \times 100 \quad (2)$$

Statistical Analysis. Data and error bars for uptake and cytotoxicity studies represent the mean ± SEM of at least 4 independent experiments. Statistical analyses for comparison between **2** and **7** were carried out using Student's t-test. Results with $p < 0.05$ were considered significantly different. Curve fitting of the cytotoxicity data was performed using Graph Pad Prism 6.0. Best nonlinear regression curve fittings were chosen by evaluating R^2, sum of square, and the standard deviation of residuals.

Confocal Fluorescence Microscopy. Two ×10^4 HeLa cells/well were seeded overnight on a 24-well plate containing a glass coverslip. Then cells were incubated for 1 h with 5 μM of **2** or **7** and 25 μg/mL of transferring alexa 488 (Molecular Probe, Life Technologies). Cells were washed 3 times in DPBS and fixed for 15 min with 4% paraformaldehyde. Cells nuclei were stained with Hoechst 33342 for 15 min. Coverslips were mounted on glass slides, and the cells were observed using a Leica SP5X confocal microscope. Images were

DOI: 10.1021/jacs.6b09504
J. Am. Chem. Soc. 2016, 138, 14488−14496

acquired using the same parameters for all samples. Quantification of red fluorescence intensity and blue fluorescence intensity was performed using Fiji, scientific image processing application based on ImageJ. Ratio of red fluorescence intensity and blue fluorescence intensity was performed for 15 nuclei per image.

■ ASSOCIATED CONTENT

Supporting Information

The Supporting Information is available free of charge on the ACS Publications website at DOI: 10.1021/jacs.6b09504.

Experimental procedures, ^{1}H NMR, ^{13}C NMR, DOSY, ESI-MS, UV−vis, Fluorescence, TEM, AFM image, zeta potential measurement, *in vitro* study, molecular modeling (PDF)

■ AUTHOR INFORMATION

Corresponding Authors

*vbriken@umd.edu

*LIsaacs@umd.edu

Notes

The authors declare the following competing financial interest(s): Lyle Isaacs holds an equity stake in Calabash Bioscience, Inc., which aims to develop (acyclic) cucurbiturils for biomedical applications.

■ ACKNOWLEDGMENTS

We thank the National Cancer Institute of the National Institutes of Heath (CA168365) for financial support.

■ REFERENCES

(1) Mitragotri, S.; Burke, P. A.; Langer, R. *Nat. Rev. Drug Discovery* **2014**, *13*, 655−672.

(2) Srinivasarao, M.; Galliford, C. V.; Low, P. S. *Nat. Rev. Drug Discovery* **2015**, *14*, 203−219.

(3) Sengupta, S.; Eavarone, D.; Capila, I.; Zhao, G.; Watson, N.; Kiziltepe, T.; Sasisekharan, R. *Nature* **2005**, *436*, 568−572.

(4) Moughton, A. O.; O'Reilly, R. K. *J. Am. Chem. Soc.* **2008**, *130*, 8714−8725. Wolinsky, J. B.; Grinstaff, M. W. *Adv. Drug Delivery Rev.* **2008**, *60*, 1037−1055. Ghang, Y.-J.; Schramm, M. P.; Zhang, F.; Acey, R. A.; David, C. N.; Wilson, E. H.; Wang, Y.; Cheng, Q.; Hooley, R. J. *J. Am. Chem. Soc.* **2013**, *135*, 7090−7093. Tian, F.; Lu, Y.; Manibusan, A.; Sellers, A.; Tran, H.; Sun, Y.; Phuong, T.; Barnett, R.; Hehli, B.; Song, F.; De Guzman, M. J.; Ensari, S.; Pinkstaff, J. K.; Sullivan, L. M.; Biroc, S. L.; Cho, H.; Schultz, P. G.; Di Joseph, J.; Dougher, M.; Ma, D.; Dushin, R.; Leal, M.; Tchistiakova, L.; Feyfant, E.; Gerber, H.-P.; Sapra, P. *Proc. Natl. Acad. Sci. U. S. A.* **2014**, *111*, 1766−1771. Zhang, F.; Zhang, S.; Pollack, S. F.; Li, R.; Gonzalez, A. M.; Fan, J.; Zou, J.; Leininger, S. E.; Pavia-Sanders, A.; Johnson, R.; Nelson, L. D.; Raymond, J. E.; Elsabahy, M.; Hughes, D. M. P.; Lenox, M. W.; Gustafson, T. P.; Wooley, K. L. *J. Am. Chem. Soc.* **2015**, *137*, 2056−2066. Yu, G.; Yu, W.; Shao, L.; Zhang, Z.; Chi, X.; Mao, Z.; Gao, C.; Huang, F. *Adv. Funct. Mater.* **2016**, DOI: 10.1002/adfm.201601770. Kim, C. S.; Duncan, B.; Creran, B.; Rotello, V. M. *Nano Today* **2013**, *8*, 439−447. Kierstead, P. H.; Okochi, H.; Venditto, V. J.; Chuong, T. C.; Kivimae, S.; Frechet, J. M. J.; Szoka, F. C. *J. Controlled Release* **2015**, *213*, 1−9.

(5) Elsabahy, M.; Heo, G. S.; Lim, S.-M.; Sun, G.; Wooley, K. L. *Chem. Rev.* **2015**, *115*, 10967−11011.

(6) Fang, J.; Nakamura, H.; Maeda, H. *Adv. Drug Delivery Rev.* **2011**, *63*, 136−151.

(7) Minotti, G.; Menna, P.; Salvatorelli, E.; Cairo, G.; Gianni, L. *Pharmacol. Rev.* **2004**, *56*, 185−229.

(8) Sun, T.; Zhang, Y. S.; Pang, B.; Hyun, D. C.; Yang, M.; Xia, Y. *Angew. Chem., Int. Ed.* **2014**, *53*, 12320−12364.

(9) Zhong, Y.-J.; Shao, L.-H.; Li, Y. A. N. *Int. J. Oncol.* **2013**, *42*, 373−383. Mitra, A. K.; Agrahari, V.; Mandal, A.; Cholkar, K.; Natarajan, C.; Shah, S.; Joseph, M.; Trinh, H. M.; Vaishya, R.; Yang, X.; Hao, Y.; Khurana, V.; Pal, D. *J. Controlled Release* **2015**, *219*, 248−268.

(10) Etrych, T.; Jelínková, M.; Říhová, B.; Ulbrich, K. *J. Controlled Release* **2001**, *73*, 89−102.

(11) Mal, P.; Breiner, B.; Rissanen, K.; Nitschke, J. R. *Science* **2009**, *324*, 1697−1699. Tranchemontagne, D. J.; Mendoza-Cortes, J. L.; O'Keeffe, M.; Yaghi, O. M. *Chem. Soc. Rev.* **2009**, *38*, 1257−1283. Clever, G. H.; Tashiro, S.; Shionoya, M. *J. Am. Chem. Soc.* **2010**, *132*, 9973−9975. Kumari, H.; Deakyne, C. A.; Atwood, J. L. *Acc. Chem. Res.* **2014**, *47*, 3080−3088. Brown, C. J.; Toste, F. D.; Bergman, R. G.; Raymond, K. N. *Chem. Rev.* **2015**, *115*, 3012−3035. Wang, W.; Chen, L.-J.; Wang, X.-Q.; Sun, B.; Li, X.; Zhang, Y.; Shi, J.; Yu, Y.; Zhang, L.; Liu, M.; Yang, H.-B. *Proc. Natl. Acad. Sci. U. S. A.* **2015**, *112*, 5597−5601. Cullen, W.; Misuraca, M. C.; Hunter, C. A.; Williams, N. H.; Ward, M. D. *Nat. Chem.* **2016**, *8*, 231−236. Wang, Q.-Q.; Gonell, S.; Leenders, S. H. A. M.; Duerr, M.; Ivanovic-Burmazovic, I.; Reek, J. N. H. *Nat. Chem.* **2016**, *8*, 225−230. Li, Z.-Y.; Zhang, Y.; Zhang, C.-W.; Chen, L.-J.; Wang, C.; Tan, H.; Yu, Y.; Li, X.; Yang, H.-B. *J. Am. Chem. Soc.* **2014**, *136*, 8577−8589. Zheng, W.; Chen, L.-J.; Yang, G.; Sun, B.; Wang, X.; Jiang, B.; Yin, G.-Q.; Zhang, L.; Li, X.; Liu, M.; Chen, G.; Yang, H.-B. *J. Am. Chem. Soc.* **2016**, *138*, 4927−4937. Young, M. C.; Holloway, L. R.; Johnson, A. M.; Hooley, R. J. *Angew. Chem., Int. Ed.* **2014**, *53*, 9832−9836. Johnson, A. M.; Wiley, C. A.; Young, M. C.; Zhang, X.; Lyon, Y.; Julian, R. R.; Hooley, R. J. *Angew. Chem., Int. Ed.* **2015**, *54*, 5641−5645. Wang, W.; Wang, Y.-X.; Yang, H. B. *Chem. Soc. Rev.* **2016**, *45*, 2656−2693. Xu, L.; Wang, Y.-X.; Chen, L.-J.; Yang, H.-B. *Chem. Soc. Rev.* **2015**, *44*, 2148−2167. McConnell, A. J.; Wood, C. S.; Neelkandan, P. P.; Nitschke, J. R. *Chem. Rev.* **2015**, *115*, 7729−7793.

(12) Cook, T. R.; Vajpayee, V.; Lee, M. H.; Stang, P. J.; Chi, K.-W. *Acc. Chem. Res.* **2013**, *46*, 2464−2474.

(13) Harris, K.; Fujita, D.; Fujita, M. *Chem. Commun.* **2013**, *49*, 6703−6712.

(14) Zheng, Y.-R.; Suntharalingam, K.; Johnstone, T. C.; Lippard, S. J. *Chem. Sci.* **2015**, *6*, 1189−1193.

(15) Yi, J. W.; Barry, N. P. E.; Furrer, M. A.; Zava, O.; Dyson, P. J.; Therrien, B.; Kim, B. H. *Bioconjugate Chem.* **2012**, *23*, 461−471.

(16) He, C.; Lu, K.; Liu, D.; Lin, W. *J. Am. Chem. Soc.* **2014**, *136*, 5181−5184.

(17) Hotze, A. C. G.; Hodges, N. J.; Hayden, R. E.; Sanchez-Cano, C.; Paines, C.; Male, N.; Tse, M.-K.; Bunce, C. M.; Chipman, J. K.; Hannon, M. J. *Chem. Biol.* **2008**, *15*, 1258−1267. Therrien, B.; Suess-Fink, G.; Govindaswamy, P.; Renfrew, A. K.; Dyson, P. J. *Angew. Chem., Int. Ed.* **2008**, *47*, 3773−3776. Vajpayee, V.; Yang, Y. J.; Kang, S. C.; Kim, H.; Kim, I. S.; Wang, M.; Stang, P. J.; Chi, K.-W. *Chem. Commun.* **2011**, *47*, 5184−5186. Grishagin, I. V.; Pollock, J. B.; Kushal, S.; Cook, T. R.; Stang, P. J.; Olenyuk, B. Z. *Proc. Natl. Acad. Sci. U. S. A.* **2014**, *111*, 18448−18453.

(18) Schmitt, F.; Freudenreich, J.; Barry, N. P. E.; Juillerat-Jeanneret, L.; Suss-Fink, G.; Therrien, B. *J. Am. Chem. Soc.* **2012**, *134*, 754−757. Yi, J. W.; Barry, N. P. E.; Furrer, M. A.; Zava, O.; Dyson, P. J.; Therrien, B.; Kim, B. H. *Bioconjugate Chem.* **2012**, *23*, 461−471.

(19) Tominaga, M.; Suzuki, K.; Kawano, M.; Kusukawa, T.; Ozeki, T.; Shakamoto, S.; Yamaguchi, K.; Fujita, M. *Angew. Chem., Int. Ed.* **2004**, *43*, 5621−5625.

(20) Bruns, C. J.; Fujita, D.; Hoshino, M.; Sato, S.; Stoddart, J. F.; Fujita, M. *J. Am. Chem. Soc.* **2014**, *136*, 12027−12034.

(21) Kim, C.; Agasti, S. S.; Zhu, Z.; Isaacs, L.; Rotello, V. M. *Nat. Chem.* **2010**, *2*, 962−966. Park, K. M.; Lee, D.-W.; Sarkar, B.; Jung, H.; Kim, J.; Ko, Y. H.; Lee, K. E.; Jeon, H.; Kim, K. *Small* **2010**, *6*, 1430−1441. Thomas, C. R.; Ferris, D. P.; Lee, J.-H.; Choi, E.; Cho, M. H.; Kim, E. S.; Stoddart, J. F.; Shin, J.-S.; Cheon, J.; Zink, J. I. *J. Am. Chem. Soc.* **2010**, *132*, 10623−10625. Li, Z.; Barnes, J. C.; Bosoy, A.; Stoddart, J. F.; Zink, J. I. *Chem. Soc. Rev.* **2012**, *41*, 2590−2605. Tarn, D.; Ashley, C. E.; Xue, M.; Carnes, E. C.; Zink, J. I.; Brinker, C. J. *Acc. Chem. Res.* **2013**, *46*, 792−801.

(22) Elci, S. G.; Jiang, Y.; Yan, B.; Kim, S. T.; Saha, K.; Moyano, D. F.; Yesilbag Tonga, G.; Jackson, L. C.; Rotello, V. M.; Vachet, R. W. *ACS Nano* **2016**, *10*, 5536−5542.
(23) Wu, Z.; Song, N.; Menz, R.; Pingali, B.; Yang, Y.-W.; Zheng, Y. *Nanomedicine* **2015**, *10*, 1493−1514.
(24) Nau, W. M.; Florea, M.; Assaf, K. I. *Isr. J. Chem.* **2011**, *51*, 559−577. Shetty, D.; Khedkar, J. K.; Park, K. M.; Kim, K. *Chem. Soc. Rev.* **2015**, *44*, 8747−8761. Wu, Y.; Lan, Y.; Liu, J.; Scherman, O. A. *Nanoscale* **2015**, *7*, 13416−13419.
(25) Masson, E.; Ling, X.; Joseph, R.; Kyeremeh-Mensah, L.; Lu, X. *RSC Adv.* **2012**, *2*, 1213−1247.
(26) Barrow, S. J.; Kasera, S.; Rowland, M. J.; del Barrio, J.; Scherman, O. A. *Chem. Rev.* **2015**, *115*, 12320−12406.
(27) Ko, Y. H.; Kim, E.; Hwang, I.; Kim, K. *Chem. Commun.* **2007**, 1305−1315.
(28) Del Barrio, J.; Horton, P.; Lairez, D.; Lloyd, G.; Toprakcioglu, C.; Scherman, O. *J. Am. Chem. Soc.* **2013**, *135*, 11760−11763. Ghale, G.; Nau, W. M. *Acc. Chem. Res.* **2014**, *47*, 2150−2159. Benyettou, F.; Zheng, X.; Elacqua, E.; Wang, Y.; Dalvand, P.; Asfari, Z.; Olsen, J.-C.; Han, D. S.; Saleh, N. i.; Elhabiri, M.; Weck, M.; Trabolsi, A. *Langmuir* **2016**, *32*, 7144−715. Benyettou, F.; Nchimi-Nono, K.; Jouiad, M.; Lalatonne, Y.; Milosevic, I.; Motte, L.; Olsen, J.-C.; Saleh, N. i.; Trabolsi, A. *Chem. - Eur. J.* **2015**, *21*, 4607−4613.
(29) Biedermann, F.; Scherman, O. A. *J. Phys. Chem. B* **2012**, *116*, 2842−2849.
(30) Bush, M. E.; Bouley, N. D.; Urbach, A. R. *J. Am. Chem. Soc.* **2005**, *127*, 14511−14517. Heitmann, L. M.; Taylor, A. B.; Hart, P. J.; Urbach, A. R. *J. Am. Chem. Soc.* **2006**, *128*, 12574−12581.
(31) Norouzy, A.; Azizi, Z.; Nau, W. M. *Angew. Chem., Int. Ed.* **2015**, *54*, 792−795.
(32) Zhang, J.; Coulston, R. J.; Jones, S. T.; Geng, J.; Scherman, O. A.; Abell, C. *Science* **2012**, *335*, 690−694. Smith, L. C.; Leach, D. G.; Blaylock, B. E.; Ali, O. A.; Urbach, A. R. *J. Am. Chem. Soc.* **2015**, *137*, 3663−3669. Bosmans, R. P. G.; Briels, J. M.; Milroy, L.-G.; de Greef, T. F. A.; Merkx, M.; Brunsveld, L. *Angew. Chem., Int. Ed.* **2016**, *55*, 8899−8903. Cavatorta, E.; Verheijden, M. L.; van Roosmalen, W.; Voskuhl, J.; Huskens, J.; Jonkheijm, P. *Chem. Commun.* **2016**, *52*, 7146−7149. Tian, J.; Chen, L.; Zhang, D.-W.; Liu, Y.; Li, Z.-T. *Chem. Commun.* **2016**, *52*, 6351−6362.
(33) Dong, N.; Xue, S.-F.; Zhu, Q.-J.; Tao, Z.; Zhao, Y.; Yang, L.-X. *Supramol. Chem.* **2008**, *20*, 663−671. Zhao, Y.; Buck, D. P.; Morris, D. L.; Pourgholami, M. H.; Day, A. I.; Collins, J. G. *Org. Biomol. Chem.* **2008**, *6*, 4509−4515. Walker, S.; Oun, R.; McInnes, F. J.; Wheate, N. J. *Isr. J. Chem.* **2011**, *51*, 616−624. Ma, D.; Zhang, B.; Hoffmann, U.; Sundrup, M. G.; Eikermann, M.; Isaacs, L. *Angew. Chem., Int. Ed.* **2012**, *51*, 11358−11362. Chen, H.; Y-W, C. J.; Li, S.; Liu, J. J.; Wyman, I.; Lee, S. M.-Y.; Macartney, D. H.; Wang, R. *RSC Adv.* **2015**, *5*, 63745−63752.
(34) Angelos, S.; Yang, Y.-W.; Patel, K.; Stoddart, J. F.; Zink, J. I. *Angew. Chem., Int. Ed.* **2008**, *47*, 2222−2226. Patel, K.; Angelos, S.; Dichtel, W. R.; Coskun, A.; Yang, Y.-W.; Zink, J. I.; Stoddart, J. F. *J. Am. Chem. Soc.* **2008**, *130*, 2382−2383. Meng, H.; Xue, M.; Xia, T.; Zhao, Y.-L.; Tamanoi, F.; Stoddart, J. F.; Zink, J. I.; Nel, A. E. *J. Am. Chem. Soc.* **2010**, *132*, 12690−12697. Thomas, C. R.; Ferris, D. P.; Lee, J.-H.; Choi, E.; Cho, M. H.; Kim, E. S.; Stoddart, J. F.; Shin, J.-S.; Cheon, J.; Zink, J. I. *J. Am. Chem. Soc.* **2010**, *132*, 10623−10625. Zhao, Y.-L.; Li, Z.; Kabehie, S.; Botros, Y. Y.; Stoddart, J. F.; Zink, J. I. *J. Am. Chem. Soc.* **2010**, *132*, 13016−13025. Ambrogio, M. W.; Thomas, C. R.; Zhao, Y.-L.; Zink, J. I.; Stoddart, J. F. *Acc. Chem. Res.* **2011**, *44*, 903−913. Yang, Y.-W. *MedChemComm* **2011**, *2*, 1033−1049. Sun, Y.-L.; Yang, B.-J.; Zhang, S. X.-A.; Yang, Y.-W. *Chem. - Eur. J.* **2012**, *18*, 9212−9216. Sun, Y.-L.; Zhou, Y.; Li, Q.-L.; Yang, Y.-W. *Chem. Commun.* **2013**, *49*, 9033−9035. Li, Q.-L.; Sun, Y.; Sun, Y.-L.; Wen, J.; Zhou, Y.; Bing, Q.-M.; Isaacs, L. D.; Jin, Y.; Gao, H.; Yang, Y.-W. *Chem. Mater.* **2014**, *26*, 6418−6431. Song, N.; Yang, Y.-W. *Chem. Soc. Rev.* **2015**, *44*, 3474−3504.
(35) Kim, H.-J.; Heo, J.; Jeon, W. S.; Lee, E.; Kim, J.; Sakamoto, S.; Yamaguchi, K.; Kim, K. *Angew. Chem., Int. Ed.* **2001**, *40*, 1526−1529.
(36) Ong, W.; Kaifer, A. E. *J. Org. Chem.* **2004**, *69*, 1383−1385.
(37) Mizuhara, T.; Saha, K.; Moyano, D. F.; Kim, C. S.; Yan, B.; Kim, Y.-K.; Rotello, V. M. *Angew. Chem., Int. Ed.* **2015**, *54*, 6567−6570. Yuan, Y.-Y.; Mao, C.-Q.; Du, X.-J.; Du, J.-Z.; Wang, F.; Wang, J. *Adv. Mater.* **2012**, *24*, 5476−5480.
(38) Li, S.-Y.; Liu, L.-H.; Rong, L.; Qiu, W.-X.; Jia, H.-Z.; Li, B.; Li, F.; Zhang, X.-Z. *Adv. Funct. Mater.* **2015**, *25*, 7317−7326.
(39) Xiao, K.; Li, Y.; Luo, J.; Lee, J. S.; Xiao, W.; Gonik, A. M.; Agarwal, R. G.; Lam, K. S. *Biomaterials* **2011**, *32*, 3435−3446.
(40) Fleischer, C. C.; Payne, C. K. *Acc. Chem. Res.* **2014**, *47*, 2651−2659.
(41) Wang, J.; Byrne, J. D.; Napier, M. E.; DeSimone, J. M. *Small* **2011**, *7*, 1919−1931.

DOI: 10.1021/jacs.6b09504
J. Am. Chem. Soc. 2016, 138, 14488−14496